

Signatures of Fractional Quantum Hall States in Topological Insulators

Dong-Xia Qu^{1*}, Y. S. Hor², and R. J. Cava³

¹*Lawrence Livermore National Laboratory, Livermore, CA 94550, USA*

²*Department of Physics, Missouri University of Science and Technology, Rolla, MO 65409, USA*

³*Department of Chemistry, Princeton University, New Jersey 08544, USA.*

(Dated: October 21, 2018)

The fractional quantum Hall (FQH) state is a topological state of matter resulting from the many-body effect of interacting electrons and is of vast interest in fundamental physics [1, 2]. The experimental observation of topological surface states (SSs) in three-dimensional bulk solids has allowed the study of a correlated chiral Dirac fermion system, which can host a single Dirac valley without spin degeneracy [3–10]. Recent theoretical studies suggest that the fractional quantum Hall effect (FQHE) might be observable in topological insulators [11, 12]. However, due to the dominant bulk conduction it is difficult to probe the strong correlation effect in topological insulators from resistivity measurements [8, 9]. Here we report the discovery of FQH states in Bi₂Te₃ from thermopower measurements. The surface thermopower is ten times greater than that of bulk, which makes possible the observation of fractional-filled Landau levels in SSs. Thermopower hence provides a powerful tool to investigate correlated Dirac fermions in topological insulators. Our observations demonstrate that Dirac topological SSs exhibit strongly correlated phases in a high magnetic field, and would enable studies of a variety of exotic fractional quantum Hall physics and other correlated phenomena in this newly discovered chiral Dirac system.

Topological insulators (TIs) are a new class of quantum states of matter with topologically protected conducting SSs, arising from the topology of the bulk electronic band structure [13–17]. There are two distinguishing features of topological surface states. One is the existence of an odd number of Dirac cones on each surface, and the other is the helical spin arrangement [5, 6, 10]. Theoretically, the relativistic nature of Dirac fermions is believed to significantly modify the electron-electron interactions, with the possibility to produce more robust ground states at the $n = 1$ Landau level (LL) in TIs than in conventional two-dimensional electron systems [20–23]. The unique spin texture and the coexistence of non-insulating bulk states also raise the intriguing question of whether TIs may host exotic FQH states owing to the non-trivial Berry's phase [16], huge Zeeman energy [24], and the screening effect from bulk carriers [11]. The potential realization of more stable non-Abelian FQH states in TIs is of practical interest for topological quantum computing [12, 25].

There have been magnetoresistance measurements at $n = 0$ and 1 LLs in (Bi_{1-x}Sb_x)₂Se₃ [9] and at $n = 4$ and 5 LLs in Bi₂Se₂Te [18]. However, the sub-integer oscillations at $n = 1$ LL in (Bi_{1-x}Sb_x)₂Se₃ can only be resolved in the second-derivative trace and their best linear fit intersects the filling-factor axis at 0 instead of 1/2, inconsistent with a Dirac spectrum. Such a property makes the exact origin of these oscillations unclear [9]. On the other hand, the FQHE in TIs is theoretically precluded in the $|n| > 1$ LLs [11], suggesting the features in Bi₂Se₂Te unlikely to be ascribed to the FQHE. So far, transport studies of FQHE in TIs have been limited to samples with

mobility below 3,000 cm²/Vs and the SS conduction is susceptible to conducting bulk states.

To explore the existence of FQH states in TIs, we present thermoelectric measurements on the Bi₂Te₃ crystals. The surface mobility of these crystals is up to 14,000 cm²/Vs [8], comparable to the Hall mobility (30,000 cm²/Vs) of high quality graphene where the FQHE has been recently discovered [26]. We first examined the dependence of thermopower S_{xx} on temperature T in both metallic and nonmetallic samples (Fig. 1, insets). Though S_{xx} shows a low- T peak in all these samples, the peak of the nonmetallic samples Q1 and Q2 is significantly stronger than that of the metallic sample M1. These observed peaks indicate the occurrence of phonon-drag effect that is expected to appear at ~ 29 K in high purity Bi₂Te₃ crystals [27]. It has been demonstrated that the phonon-drag thermopower from a two-dimensional (2D) conducting layer on a three-dimensional (3D) crystal can display giant quantum oscillations due to the phonon intra- and inter-LL scattering in the presence of a strong magnetic field. In such a 3D system, surface electrons are dragged by non-equilibrium 3D phonons of the whole specimen, while in a purely 2D system such as graphene, electrons of a wavevector k can only interact with 2D phonons of a wavevector $q \leq 2k$. In addition, the bulk thermopower is considerably suppressed due to the existence of two types of bulk carriers with opposite signs [8]. Therefore, we expect that the magneto-thermopower of SSs is orders of magnitude larger than that of bulk in the high field limit. The thermopower measurement thus provides a powerful tool to elucidate the nature of the topological SSs that is difficult to be probed by the conductance measurement.

*All correspondence should be addressed to D. Qu (qu2@llnl.gov)

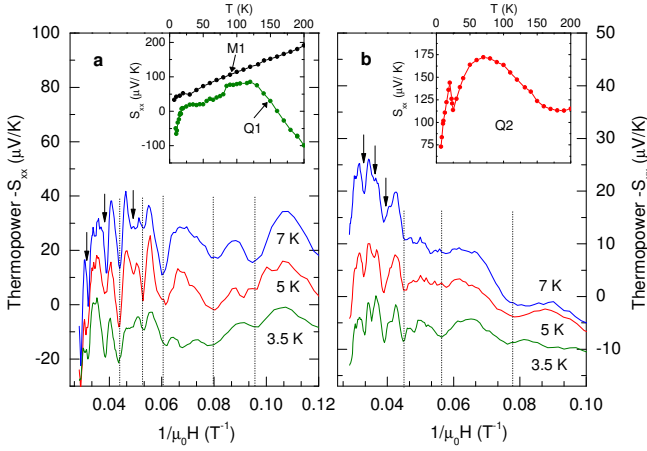


FIG. 1: Magneto-thermopower in high magnetic fields. (a) The thermopower response $-S_{xx}$ versus $1/H$ in sample Q1 at temperatures $T = 3.5, 5,$ and 7 K. (b) $-S_{xx}$ versus $1/H$ in sample Q2. The insets show the T dependence of the thermopower profiles in samples Q1 and M1 in (a) and in sample Q2 in (b). The arrows mark the sub-integer dips resolved in $1/H > 0.06 \text{ T}^{-1}$. The dashed lines indicate the oscillating minima in the low field regime.

Figure 1, a and b, show the thermopower response $-S_{xx}$ versus the inverse magnetic field $1/H$ in samples Q1 and Q2, respectively. Large LL oscillations begin to emerge at $H > 8$ T and their amplitude becomes smaller as T decreases from 7 to 3.5 K. A prominent feature of these oscillations is that at $1/H < 0.06 \text{ T}^{-1}$ sharp dips (black arrows) appear, with an aperiodic spacing smaller than the oscillating structure in the low field limit.

It is illuminating to compare the oscillations in $-S_{xx}$ and the Shubnikov-de Hass (SdH) effect in the conductance tensor G_{xx} , which was confirmed to arise from the 2D SSs in the previous study [8]. As shown in Fig. 2, a and b, the extrema in $-\Delta S_{xx}$ coincide with the extrema in ΔG_{xx} . This occurs because both $-S_{xx}$ ($S_{xx} < 0$ for electron-like carriers) and σ_{xx} peak when the Fermi level (E_F) aligns with each LL, whereas vanish when E_F lies between LLs. Furthermore, we observe pronounced LL splitting near $1/H = 0.061, 0.102,$ and 0.142 T^{-1} (gray dashed lines in Fig. 2b). This splitting indicates that the degeneracy is lifted between top (+) and bottom (-) surfaces. Similar effect has been seen in strained HgTe 3D TIs [19]. Here, a weak Te composition gradient in Bi_2Te_3 breaks the inversion symmetry and generates displaced Dirac points (see the inset of Fig. 2a). By cleaving the crystal into bulk samples with a thickness $t = 20 \sim 100 \mu\text{m}$, we obtain slightly different surface carrier densities, which then leads to two sets of Landau filling factor ν in one piece of sample (Fig. 2c). Hence, we can pinpoint the top and bottom surface index fields B_{ν^+} and B_{ν^-} from the periodic spacing of strong (black dashed lines) and weak (grey dashed lines) minima in ΔG_{xx} for sample Q2. Similar results were observed in sample Q1, with its bottom surface cleaved adjacent to the top surface of sample Q2. As shown below, the extracted bottom sur-

face carrier concentration in Q1 is almost the same as the top surface carrier concentration in Q2. The Fermi energy levels relative to the Dirac point in samples Q1 and Q2 are sketched in Fig. 2d.

In terms of the carrier concentration n_e on one surface, B_ν is related to ν by

$$B_\nu = \frac{n_e \phi_0}{(\nu - \gamma)} \quad (1)$$

where $\phi_0 = h/e$ is the magnetic flux quanta, h Planck's constant, e the charge of electron, and γ the filling factor shift. A shift with $\gamma = 0$ corresponds to a conventional spectrum, whereas a deviation from the zero-shift with $\gamma = 1/2$ implies a Dirac spectrum. The $1/2$ arises from the $n = 0$ LL at the Dirac point. In the following, we label the filling factors as ν^s , where $s = \pm$ indexes the top and bottom SSs. With the $B_{\nu^s}^{-1}$ identified in both $-S_{xx}$ and ΔG_{xx} , we plot them against integers (triangles and circles in Fig. 3, a and b). The slopes of the linear-fit to the data yield the carrier concentration $n_e = 9.27 (7.61) \times 10^{11}$ and $7.37 (5.92) \times 10^{11} \text{ cm}^{-2}$, with the Fermi wavevector $k_F = 0.034 (0.031)$ and $0.030 (0.027) \text{ \AA}^{-1}$, for the top (bottom) SSs in samples Q1 and Q2, respectively. The linear-fit intercepts the ν axis at $\gamma = 0.45 \pm 0.02$ in Q1 and 0.67 ± 0.02 in Q2, consistent with a Dirac dispersion. Hence, we are again convinced that the 2D Dirac states give rise to the LL indexing shown in Fig. 2. Furthermore, the weak-field Hall anomaly provides an independent measurement of the average surface wavevector. The value of k_F derived from surface Hall conductance is in reasonable agreement with the quantum oscillation analysis.

We then illustrate the fine structure of $-S_{xx}$ in the range of $1 < \nu < 2$ for samples Q1 and Q2 (Fig. 3, c and d). We observed narrow, reproducible minima at the fields B_{ν^s} (dashed lines) with $\nu^s = 5/3^\pm$. In addition to the minima at $\nu^s = 5/3^\pm$, a valley-like structure at $\nu^s = 9/5^\pm$ is discernable in Q1, and the dip at $\nu^s = 9/5^+$ becomes prominent in Q2 as the temperature decreases. As seen in Fig. 3, a and b, the fractional Landau fillings lie on a straight line with the integer ones. To examine the oscillating profiles of the most pronounced sub-integer structures, we plot the $-S_{xx}$ versus the filling factor calculated as $\nu = n_e \phi_0 B^{-1} + \gamma$ (Fig. 4, a and b). The $-S_{xx}(\nu)$ traces obtained at various n_e are almost overlapped, and their minima are all located around $\nu = 1.67 \pm 0.02$ (traces are displaced for clarity). Both features strongly suggest that the observed high-field structures are associated with the FQH states at $n = 1$ LL. Based on the theory of theomopower in the QHE regime, a minimum in σ_{xx} should accompany a minimum in thermopower. As shown in Fig. 2b (black arrows), two sub-integer dips are clearly resolved in $\Delta \sigma_{xx}$ with ν^s close to $\pm 5/3$. Noting that for conventional 2D electron gas in the FQH regime, ρ_{xy} should be quantized with $(\nu e^2/h)^{-1}$ at filling factor ν . Unfortunately, the present of the bulk conduction channel does not allow us to measure exact Hall magnitude. Even in most resis-

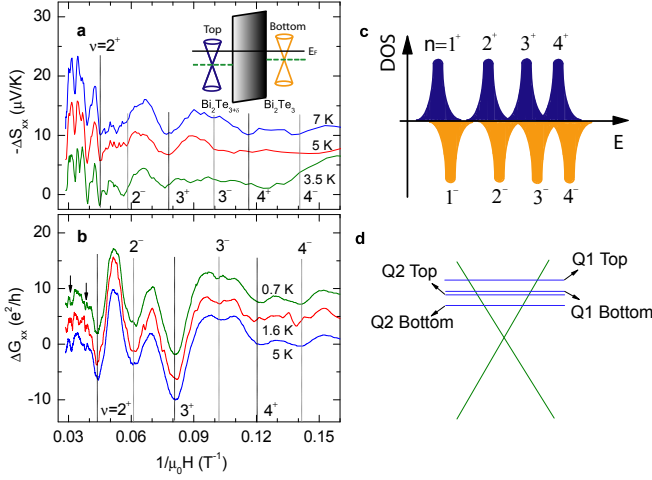


FIG. 2: Quantum oscillations from integer Landau level. (a) The oscillating component of thermopower $-\Delta S_{xx}$, obtained by subtracting a smooth background from $-S_{xx}$ in sample Q2. The inset sketches the Dirac cone position on both surfaces at the existence of a slightly Te composition gradient in bulk samples. The Fermi energy E_F is fixed across the bulk sample. (b) Longitudinal conductivity ΔG_{xx} with a smooth background subtracted is plotted against $1/H$ at selected temperatures $T = 0.7, 1.6,$ and 5 K in the same sample. Dashed vertical lines mark the minima in $-\Delta S_{xx}$ and ΔG_{xx} , which are consistent with integer ν of top (+) and bottom (-) Fermi surface. The variation of Dirac point positions in two surfaces with a constant Fermi level E_F is shown as an inset in (a). (c) Sketch showing how the composition gradient induces the top and bottom Landau level displacement. (d) Illustration of the energy difference between the Fermi energy level E_F (short lines) and the Dirac point of top or bottom surface states in samples Q1 and Q2.

tive TIs, Hall quantization is obscured by dominate bulk contribution and no quantized Hall plateaus have so far been observed.

In spite of the limited data set, we may roughly estimate the lower bound of the gap energy of the $5/3$ state ($\Delta_{5/3}$) from the T dependence of the thermopower and resistivity minima, both of which scale as $e^{-\Delta/2T}$. As shown in Fig. 2b and Fig. 3, c and d, the $5/3^+$ state persists until 5 K, indicating $\Delta_{5/3} > 5$ K. This value is more than an order of magnitude larger than the corresponding gap ($\Delta_{8/3}$) in the GaAs system with a much higher mobility [30], but comparable to the gap in graphene with a similar mobility [26]. This is not surprising because the $n = 1$ LL in the topological SSs is a mixture of the $n = 0$ and 1 LLs in non-relativistic systems. It makes the FQH states in the $n = 1$ LL in the Dirac system more robust than those in the GaAs system [11, 20–23, 31, 32]. Compared with graphene, the surface states in Bi_2Te_3 has only one Dirac valley with no spin degeneracy, analogous to a completely four-fold degeneracy lifted graphene system where the FQH states do not mix between spin- and valley-bands. Moreover, the helical spin texture of topological SSs and the presence of conductive bulk states may lead to enhanced effective Coulomb in-

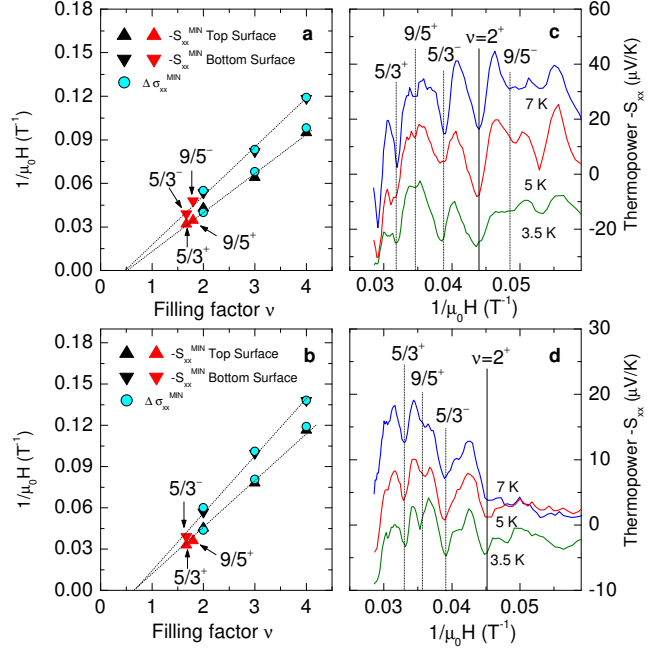


FIG. 3: Identification of fractional quantum Hall states. The left panel shows the $1/H$ positions of the $-S_{xx}$ and ΔG_{xx} minima versus the filling factor ν in sample Q1 (a) and sample Q2 (b). The black and red triangles represent the integer and fractional fillings, respectively. The right panel shows the fine structure of thermopower response $-S_{xx}$ versus $1/H$ for $1/H < 0.06$ T^{-1} in sample Q1 (c) and sample Q2 (d). Identified minima correspond to the fractional-filling factors illustrated as the vertical dashed lines. Note that the minima at $\nu = 5/3^+$ and $5/3^-$ are much stronger than those at $\nu = 9/5^+$ and $9/5^-$.

teractions, rendering the FQH states even more robust in TIs [11].

We next extract the surface thermopower S_{xx}^s from the observed thermopower response. The measured thermopower tensor S_{ij} can be expressed as the sum,

$$S_{ij} = \sum_{k=x,y} \rho_{ik} \left(\alpha_{kj}^b + \frac{\alpha_{kj}^s}{t} \right) \quad (2)$$

where ρ_{ij} is the total resistivity tensor, $\alpha_{ij}^l = \sum_{k=x,y} \sigma_{ik}^l S_{kj}^l$ with $l = b$ or s , the bulk or surface thermoelectric conductivity tensor, and σ_{ij}^l the bulk or surface conductivity tensor. Since $\rho_{xx} \gg \rho_{yy}$, $\sigma_{xx}^b \gg \sigma_{xy}^b$, $\sigma_{xx}^s \gg \sigma_{xy}^s$, and $\sigma_{xx} \gg \sigma_{xx}^s$ for nonmetallic Bi_2Te_3 in the high-field regime, S_{xx} can be approximated as

$$S_{xx} = S_{xx}^b + \frac{1}{t} \rho_{xx} G_{xx}^s S_{xx}^s \quad (3)$$

where S_{xx}^b is the bulk thermopower and G_{xx}^s the surface conductance. The bulk thermopower only gives rise to a featureless background. The $\rho_{xx} G_{xx}^s / t$ term can be obtained from the resistivity measurements. We find that the maximum magnitude of $\rho_{xx} G_{xx}^s / t \sim 0.027$ and 0.01 in Q1 and Q2, respectively. From Eq. (3), we can extract the $-S_{xx}^s$ versus H in Q1 and Q2 (Fig. 4, c and

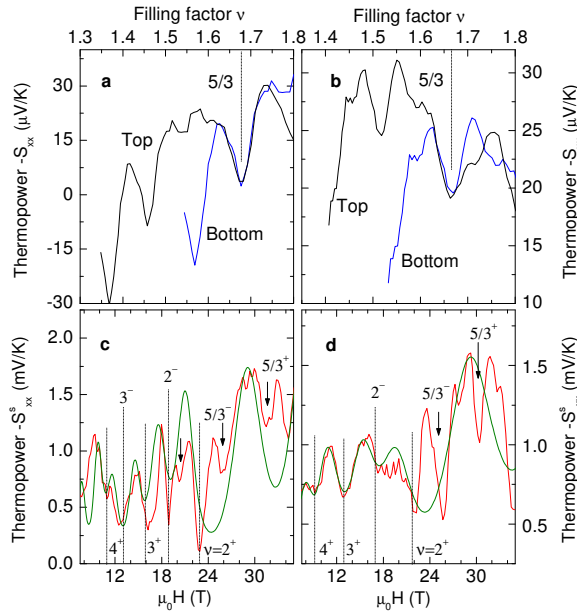


FIG. 4: Characteristics of the $\nu = 5/3$ state and the numerical simulation of the surface thermopower. (a) $-S_{xx}$ as a function of the filling factor $\nu = n_e \phi_0 B^{-1} + \gamma$ in sample Q1 at 7 K. (b) $-S_{xx}$ versus ν in sample Q2 at 7 K. In (a) and (b) curves are vertically offset for clarity. (c), (d) The surface thermopower $-S_{xx}^s$ obtained by removing a smooth background contributed from S_{xx}^b in sample Q1 (c) and sample Q2 (d) at 5 K. The green curve is the fit to $-S_{xx}^s$ based on the Dirac fermion and 3D phonon interaction model. The H positions at the integer-filling factors are marked by dotted lines. The fractional structures resolved at $\nu^s < 2^-$ are indicated by arrows.

d, red curves). The peak magnitude of $-S_{xx}^s$ is in the range of $0.5 - 2.0 \text{ mV K}^{-1}$, which is more than an order of magnitude higher than that of the bulk $\sim 30 \text{ } \mu\text{V K}^{-1}$ at 5 K. Unlike conventional 2D systems where the thermopower magnitude roughly displays a linear field dependence [28], the surface thermopower at higher order LLs such as $n = 4$ is comparable or even greater than that of lower LLs ($n = 3$). This giant oscillating magnitude

and the specific field profile of the surface thermopower can be understood within the scenario of the 2D Dirac electron and 3D phonon interaction.

Because of the relativistic dispersion of topological surface states, the wave function Ψ_n of a Dirac electron in the n th LL is the superposition of the n th and $(n - 1)$ th LL wave functions of a non-relativistic electron. The mixture nature of the wave function significantly modifies the electron-phonon matrix element in the $n \geq 1$ LLs, leading to a thermopower profile different from an ordinary 2D system.

Using a general model given in ref. 29 and the wave function for topological SSs [24], we numerically simulate the thermopower induced by the integer Landau quantization in Q1 and Q2, with the phonon mean free path treated as a fitting parameter (Fig. 4, c and d, green curves). We include the average LL broadening width $\Gamma = 3.5$ and 7 meV for Q1 and Q2, respectively. The simple electron-phonon interaction model (Eq. S5) does not capture the fractional features, as FQHE is not included in the model. However, it reproduces the index field position and the oscillation magnitude from the integer Landau quantization. This suggests that the observed giant integer Landau oscillations can be explained by 2D Dirac fermion and 3D phonon interaction. A more comprehensive FQHE framework is needed to model the fractional-filling states in thermopower response.

By performing thermopower measurements, we have resolved fractional Landau quantization of SSs at $\nu = 5/3$ and $9/5$. The observed gap energy at the $5/3$ state is ten times larger than that of the non-relativistic electron systems. The demonstration of the FQH states in the topological surface bands opens the door to future studies of fractional quantum Hall effect physics in the topological insulator, which is expected to display strong correlation effects between chiral Dirac fermions.

The authors would like to thank N. P. Ong, F. D. Haldane, L. Fu, and C.-X. Liu for helpful discussion.

-
- [1] Tsui, D. C., Stormer, H. L. & Gossard, A. C. Two-dimensional magnetotransport in the extreme quantum limit. *Phys. Rev. Lett.* **48**, 1559-1562 (1982).
 - [2] Jain, J. K. The composite fermion: a quantum particle and its quantum fluids. *Phys. Today* **53**, 39-45 (2000).
 - [3] Hasan, M. Z. & Kane, C. L. Colloquium: Topological insulators. *Rev. Mod. Phys.* **82**, 3045-3067 (2010).
 - [4] Hsieh, D. *et al.* A topological Dirac insulator in a quantum spin Hall phase. *Nature* **452**, 970-974 (2008).
 - [5] Hsieh, D. *et al.* Observation of unconventional quantum spin textures in topological insulators. *Science* **323**, 919-922 (2009).
 - [6] Roushan, P. *et al.* Topological surface states protected from backscattering by chiral spin texture. *Nature* **460**, 1106-1109 (2009).
 - [7] Chen, Y. L. *et al.* Experimental Realization of a Three Dimensional Topological Insulator, Bi_2Te_3 . *Science* **325**, 178-181 (2009).
 - [8] Qu, D.-X. *et al.* Quantum oscillations and Hall anomaly of surface states in the topological insulator Bi_2Te_3 . *Science* **329**, 821-824 (2010).
 - [9] Analytis, J. G. *et al.* Two-dimensional surface state in the quantum limit of a topological insulator. *Nat. Phys.* **6**, 960-964 (2010).
 - [10] Xia, Y. *et al.* Observation of a large-gap topological-insulator class with a single Dirac cone on the surface. *Nature Phys.* **5**, 398-402 (2009).
 - [11] DaSilva, A. M. The stability of the fractional quantum Hall effect in topological insulators. *Solid State Communications* **151**, 1444-1446 (2011).
 - [12] Moore, J. E. The birth of topological insulators. *Nature* **464**, 194-198 (2010).

- [13] Kane, C. L. & Mele, E. J. Z_2 topological order and the quantum spin Hall effect. *Phys. Rev. Lett.* **95**, 146802 (2005).
- [14] Bernevig, B. A. & Zhang, S.-C. Quantum spin Hall effect. *Phys. Rev. Lett.* **96**, 106802 (2006).
- [15] Moore, J. E. & Balents, L. Topological invariants of time-reversal-invariant band structures. *Phys. Rev. B* **75**, 121306 (R) (2007).
- [16] Fu, L. & Kane, C. L. Topological insulators with inversion symmetry. *Phys. Rev. B* **76**, 045302 (2007).
- [17] Qi, X.-L., Hughes, T. L. & Zhang, S.-C. Topological field theory of time-reversal invariant insulators. *Phys. Rev. B* **78**, 195424 (R) (2008).
- [18] Xiong, J. *et al.* Quantum Oscillations in a Topological Insulator $\text{Bi}_2\text{Te}_2\text{Se}$ with Large Bulk Resistivity ($6 \Omega\text{cm}$). arXiv:1101.1315v1, to appear in *Physica E*.
- [19] Brune, C. *et al.* Quantum Hall Effect from the Topological Surface States of Strained Bulk HgTe . *Phys. Rev. Lett.* **106**, 126803 (2011).
- [20] Goerbig, M. O., Moessner, R. & Doucot, B. Electron interactions in graphene in a strong magnetic field. *Phys. Rev. B* **74**, 161407 (2006).
- [21] Yang, K., Sarma, S. D. & MacDonald, A. H. Collective modes and skyrmion excitations in graphene $\text{SU}(4)$ quantum Hall ferromagnets. *Phys. Rev. B* **74**, 075423 (2006).
- [22] Apalkov, V. M. & Chakraborty, T. Fractional quantum Hall states of Dirac electrons in Graphene. *Phys. Rev. Lett.* **97**, 126801 (2006).
- [23] Toke, C. *et al.* Fractional quantum Hall effect in graphene. *Phys. Rev. B* **74**, 235417 (2006).
- [24] Liu, C.-X. *et al.* Model Hamiltonian for topological insulators. *Phys. Rev. B* **82**, 045122 (2010).
- [25] Nayak, C. *et al.* Non-Abelian anyons and topological quantum computation. *Rev. Mod. Phys.* **80**, 1083-1159 (2008).
- [26] Dean, C. R. *et al.* Multicomponent fractional quantum Hall effect in graphene. *Nature Phys.* **7**, 693696 (2011).
- [27] Kittel, C. *Introduction to Solid State Physics* (John Wiley & Sons, NY, 1996).
- [28] Fletcher, R. *et al.* Thermoelectric properties of $\text{GaAs-Ga}_{1-x}\text{Al}_x\text{As}$ heterojunctions at high magnetic fields. *Phys. Rev. B* **33**, 7122 (1986).
- [29] Lyo, S. K. Magnetoquantum oscillations of the phonon-drag thermoelectric power in heterojunctions. *Phys. Rev. B* **40**, 6458 (1989).
- [30] Pan, W. *et al.* Experimental studies of the fractional quantum Hall effect in the first excited Landau level. *Phys. Rev. B* **77**, 075307 (2008).
- [31] Bolotin, K. I. *et al.* Observation of the fractional quantum Hall effect in graphene. *Nature* **462**, 196-199 (2009).
- [32] Du, X. *et al.* Fractional quantum Hall effect and insulating phase of Dirac electrons in graphene. *Nature* **462**, 192-195 (2009).